The DFK electronic coupling model does provide a reasonable account of the positions and parities of the IR and near-IR transitions in the Creutz–Taube complex and has some relevance to the MCD spectra. The relative intensities of the transitions do however pose a serious problem and may indicate a limit to the validity of the simple two-center approach in the Creutz–Taube ion. MCD and deuteration studies in the near-IR and IR regions,[4,15] along with singe-crystal polarized studies,[4] have established substantial non-interion- (*Z*-) polarized and vibronically induced intensity. The vibronically *induced* (parity-forbidden) intensity problem has not as yet been accessed theoretically for mixed-valence systems. Experimentally, this process is active in a number of mixed-valence systems and seems to involve proton modes specifically. Ammine stretch and deformation modes couple very strongly to single-ion transitions in Ru(III) monomers.[16] We are currently making further MCD and absorption measurements of a range of strongly coupled mixed-valence dimers, including the osmium analogue of the Creutz–Taube ion, and are recording spectra of analogous monomer materials in Nafion films in order to establish further the generality of these phenomena.

Acknowledgment. E.K. thanks Professor P. N. Schatz for a copy of a manuscript prior to publication[19] and Drs. L. Dubicki and P. Bernhardt for useful discussions.

Registry No. PTFE, 9002-84-0; Creutz–Taube ion, 35599-57-6; Nafion, 39464-59-0.

Contribution from the Laboratoire de Chimie Théorique (UA 506), Université de Paris-Sud, 91405 Orsay Cedex, France, and Department of Chemistry, North Carolina State University, Raleigh, North Carolina 27695-8204

Electronic Structure of Nb_3X_4 Type Compounds

Enric Canadell*† and Myung-Hwan Whangbo*‡

Received October 7, 1985

Tight-binding band calculations were performed on Nb_3S_4 and model Nb_2S_6 chains to examine how the electronic structure of Nb_3S_4 is related to its crystal structure. The low-lying d-block bands of Nb_3S_4 were found to be similar in nature to the t_{2g} subbands of Nb_2S_6 chains of which Nb_3S_4 consists. The low $n(e_f)$ values of Nb_3X_4 compounds originate from both strong through-space metal–metal 1,2-interactions and good through-bond metal–metal 1,3-interactions within each Nb_2X_6 chain. On the basis of the band electronic structure and the density of states of Nb_3S_4 calculated in the present work, it was found that the Fermi surfaces and the $n(e_f)$ values of the Nb_3X_4 and Ti_3X_4 lattices can be significantly modified by alkali-metal intercalation.

The crystal structure of triniobium tetrachalcogenides Nb_3X_4 (X = S, Se, Te),[1] discovered more than two decades ago, consists of zigzag Nb chains parallel to the *c* axis. Each zigzag Nb chain is linked to adjacent chains via chalcogen atoms to form hexagonal channels parallel to the *c* axis. Recently, Nb_3X_4 compounds were found to have a number of interesting properties such as superconductivity,[2] an unusual electrical transport property,[3a-c] a charge density wave,[3d] and alkali-metal intercalation.[4] Available band electronic structure studies on Nb_3X_4[5] showed that Nb_3X_4 compounds are pseudo one-dimensional metals and that their densities of states at the Fermi level, $n(e_f)$, are small. These studies were primarily concerned with the electrical transport properties of Nb_3X_4[5,6] and did not examine how the band electronic structures of Nb_3X_4 are related to their crystal structures. Thus in the present study, the latter question was probed in some detail by performing tight-binding band calculations[7] on Nb_3S_4 and Nb_2S_6 model chains. The atomic parameters employed in our study are summarized in Table I.

Results and Discussion

A. Crystal Structure. A projected view of Nb_3S_4 along the *c* axis is shown in **1**, where empty and filled circles differ in their heights by $c/2$ along the *c* axis. This diagram, **1**, emphasizes the presence of triangular Nb clusters.[1,8] Each Nb atom is surrounded by six sulfur atoms that form a distorted octahedron, as can be seen from the Nb–S bond lengths shown in **1**. The triangular Nb clusters are linked via sulfur atoms in such a way that there occur two kinds of sulfur atoms, one surrounded by six Nb atoms and the other surrounded by four Nb atoms. The latter sulfur atoms form hexagonal channels parallel to the *c* axis, which are responsible for alkali-metal intercalation of Nb_3X_4.[4]

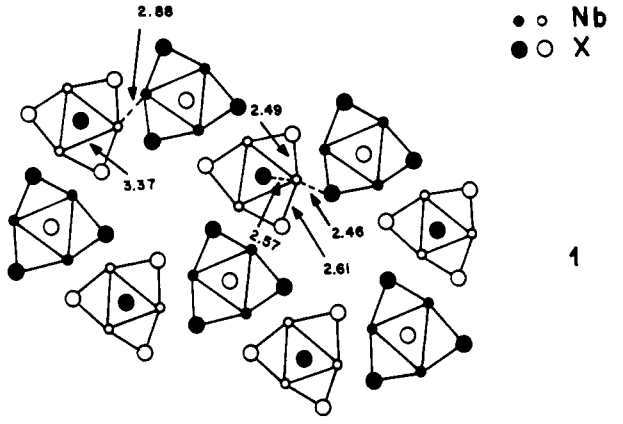

1

As also indicated in **1**, the shortest Nb–Nb distance is 3.37 Å within a triangular Nb cluster but 2.88 Å between adjacent

† Université de Paris-Sud.
‡ North Carolina State University.

(1) (a) Selte, K.; Kjekshus, A. *Acta Crystallogr.* **1964**, *17*, 1568. (b) Ruysink, A. F. J.; Kadijk, F.; Wagner, A. J.; Jellinek, F. *Acta Crystallogr., Sect. B: Struct. Crystallogr. Cryst. Chem.* **1968**, *B24*, 1614.
(2) Amberger, E.; Polborn, K.; Grimm, P.; Dietrich, M.; Obst, B. *Solid State Commun.* **1978**, *26*, 943.
(3) (a) Ishihara, Y.; Nakada, I. *Solid State Commun.* **1983**, *45*, 129. (b) Ishihara, Y.; Nakada, I.; Suzuki, K.; Ichihara, M. *Solid State Commun.* **1984**, *50*, 657. (c) Rashid, M. H.; Sellmyer, D. J. *Phys. Rev. B: Condens. Matter* **1984**, *29*, 2359 (d) Suzuki, K.; Ichihara, M.; Nakada, I.; Ishihara, Y. *Solid State Commun.* **1984**, *52*, 743.
(4) (a) Schöllhorn, R. *Angew. Chem., Int. Ed. Engl.* **1980**, *19*, 983. (b) Schöllhorn, R.; Kuhlmann, R.; Besenhard, J. O. *Mater. Res. Bull.* **1976**, *11*, 83. (c) Schöllhorn, R.; Schramm, W.; Fenske, D. *Angew. Chem., Int. Ed. Engl.* **1980**, *19*, 492. (d) Schöllhorn, R.; Schramm, W. *Z. Naturforsch., B: Anorg. Chem., Org. Chem.* **1979**, *34B*, 697. (e) Boller, H.; Klepp, K. *Mater. Res. Bull.* **1983**, *18*, 437.
(5) (a) Oshiyama, A. *Solid State Commun.* **1982**, *43*, 607. (b) Oshiyama, A. *J. Phys. Soc. Jpn.* **1983**, *52*, 587. (c) Bullet, D. W. *J. Solid State Chem.* **1980**, *33*, 13.

0020-1669/86/1325-1488$01.50/0

Table I. Exponents ζ_μ and Valence-Shell Ionization Potentials $H_{\mu\mu}$ for Slater Type Orbitals χ_μ[a,b]

χ_μ	ζ_μ	ζ_μ'	$H_{\mu\mu}$, eV
Nb 5s	1.90		−10.10
Nb 5p	1.85		−6.86
Nb 4d	4.08 (0.6401)	1.64 (0.5516)	−12.10
S 3s	1.817		−20.00
S 3p	1.817		−13.30

[a] The d orbitals of Nb are given as a linear combination of two Slater type orbitals, and each is followed by the weighting coefficient in parentheses.[13] [b] A modified Wolfsberg–Helmholz formula was used to calculate $H_{\mu\nu}$.[14]

clusters. The Nb–Nb distance of 2.88 Å is compatible with a single Nb–Nb bond length,[9] so that the structure of Nb_3S_4 can be better described by **2**, where emphasis is placed upon the

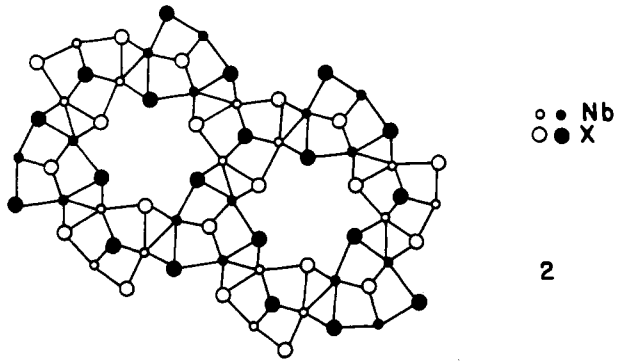

2

presence of zigzag Nb chains that are linked via sulfur atoms. Therefore a structural building block containing one zigzag Nb chain may be considered as the Nb_2S_6 chain **3**. Such Nb_2S_6

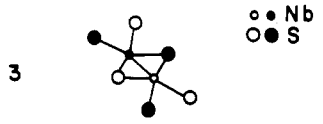

3

chains lead to the Nb_3S_4 structure **2** by sharing their sulfur atoms. The Nb_2S_6 chain **3** (hereafter referred to as real Nb_2S_6 chain) may be regarded as distorted from an ideal Nb_2S_6 chain **4**, which

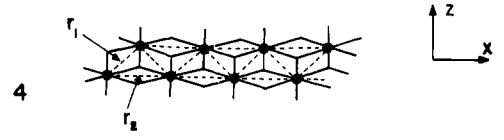

4

is simply derived from regular NbS_6 octahedra upon sharing four edges. The Nb_2S_6 chain **4** may also be obtained by fusing two trans-edge-sharing NbS_4 chains **5**. Namely, the chain **4**, and

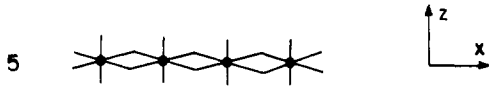

5

hence **3** as well, consists of two NbS_4 subchains. Conversion of **4** into **3** is achieved when every Nb–Nb contact between subchains (i.e., r_1) is shortened while every Nb–Nb contact within each subchain (i.e., r_2) is kept long. In real chain **3** the short Nb–Nb distance is 2.88 Å between subchains but 3.37 Å within each subchain.

(6) Ishihara, Y.; Nakada, I. *Solid State Commun.* **1982**, *42*, 579.
(7) (a) Whangbo, M.-H.; Hoffmann, R. *J. Am. Chem. Soc.* **1978**, *100*, 6093. (b) Whangbo, M.-H.; Hoffmann, R.; Woodward, R. B. *Proc. R. Soc. London, A* **1979**, *366*, 23.
(8) Simon, A. *Angew. Chem. Int. Ed. Engl.* **1981**, *20*, 1.
(9) (a) von Schnering, H. G.; Wohrle, H.; Schafer, H. *Naturwissenschaften* **1961**, *48*, 159. (b) Simon, A.; von Schnering, H. G. *J. Less-Common Met.* **1966**, *11*, 31. (c) Taylor, D. R.; Calabrese, J. C.; Larsen, E. M. *Inorg. Chem.* **1977**, *16*, 721. (d) Dahl, L. F.; Wampler, D. L. *Acta Crystallogr.* **1962**, *15*, 903. (e) Schafer, H.; Dohmann, D.-D. *Z. Anorg. Allg. Chem.* **1961**, *311*, 134. (f) Seabaugh, P. W.; Corbett, J. D. *Inorg. Chem.* **1965**, *4*, 176.

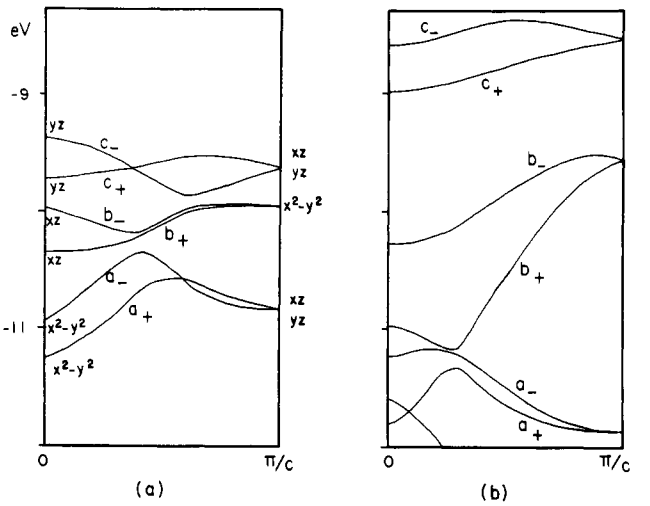

Figure 1. Low-lying *d*-block bands of Nb_2S_6 chains: (a) t_{2g} subbands of ideal Nb_2S_6 chain; (b) t_{2g} subbands of real Nb_2S_6 chain.

B. Band Electronic Structure. The electronic structure of Nb_3S_4 can be easily understood in terms of its building blocks, Nb_2S_6 chains **3**. It is convenient to describe the electronic structure of real Nb_2S_6 chain **3** in terms of that of ideal Nb_2S_6 chain **4**. Thus in the following, we will discuss first ideal chain **4**, then real chain **3**, and finally Nb_3S_4.

B.1. Ideal Nb_2S_6 Chain. Ideal chain **4** may be constructed from regular NbS_6 octahedra with the Nb–S bond length of 2.45 Å, the shortest Nb–S bond present in **3**. Then in **4** all Nb–Nb contacts either between subchains or within each subchain become 3.46 Å. This distance is long compared with the shortest Nb–Nb distance of 2.88 Å between subchains but comparable with that of 3.37 Å within each subchain in **3**.

Figure 1a shows the six low-lying d-block bands (a_+, a_-, b_+, b_-, c_+, c_-) of **4** that originate from t_{2g} levels of each metal. As shown in **6–8**, these t_{2g} subbands are largely constructed from the

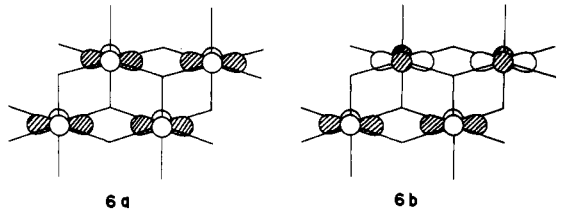

6a **6b**

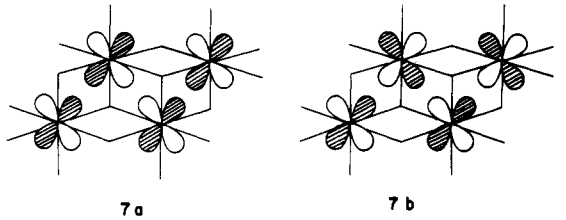

7a **7b**

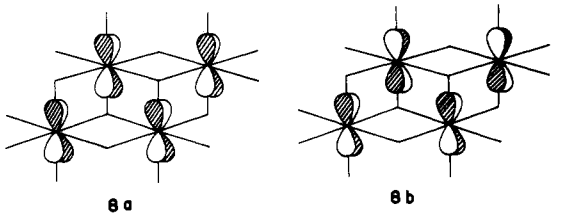

8a **8b**

$x^2 - y^2$, xz, and yz orbitals of each metal. **6a**, **6b**, **7a**, **7b**, **8a**, and **8b** show the major nodal properties of bands a_+, a_-, b_+, b_-, c_+, and c_- at $k = 0$, respectively.

As k varies from 0 to π/c, the t_{2g} subbands undergo a seemingly complicated change in character. The major orbital components of these bands at π/c, which occur pairwise, are shown in **9–11**.

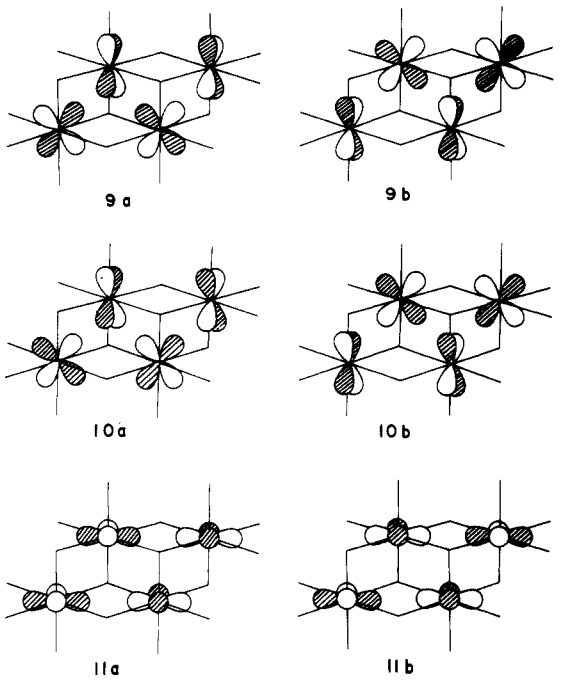

The nodal properties of a_+ and a_- at π/c are given by **9a** and **9b**, which have good through-space interactions between xz orbitals of one subchain and yz orbitals of the other subchain. The major nodal properties of c_+ and c_- at π/c are described by **10a** and **10b**, which have good through-space antibonding interactions between metal atoms of two subchains.

The major orbital components of b_+ and b_- at π/c are represented by **11a** and **11b**. Band orbitals **11** are higher in energy than **6** due primarily to the difference in the through-bond interactions provided by bridging sulfur atom p orbitals in the subchains (for simplicity, sulfur p orbitals are not shown in **6**–**11**).[10] Orbitals **11** lie between **9** and **10** at $k = \pi/c$, because through-space interactions of xz orbitals of one subchain with yz orbitals of the other subchain are strong.

Around the zone end, Figure 1a shows that the b_+ and b_- bands are nearly flat and close in energy to the c_+ and c_- bands. This arises from the fact that, around $k = \pi/c$, orbitals **10** and **11** intermix. The extent of this orbital mixing is diminished when orbitals **10** are raised in energy with respect to orbitals **11**.

B.2. Real Nb_2S_6 Chain. Figure 1b shows the t_{2g} subbands of real Nb_2S_6 chain **3**. As already noted, this chain structure is obtained from **4** primarily upon shortening every Nb–Nb distance between the two subchains. This distortion enhances the through-space metal–metal interactions between the two subchains of **4**, so that orbitals **9** are lowered but orbitals **10** are raised in energy. Thus the a_+ and a_- bands are lower in energy, while the c_+ and c_- bands are higher, in **3** than in **4**. In real chain **3**, the two bands a_+ and a_- describe metal–metal bonding interactions in the two Nb–Nb contacts per unit cell across the subchains, while bands c_+ and c_- describe the corresponding antibonding interactions. Thus when the a_+ and a_- bands are both doubly occupied, there occur two single Nb–Nb bonds per unit cell.

Note that the a_+ and a_- bands, and the c_+ and c_- bands as well, are rather flat along the chain direction. This is so because those bands describe interactions between metal–metal bonds across the subchains. On the other hand, the b_+ and b_- bands are somewhat more dispersive in **3** than in **4**. This is due to the fact that in **3** orbitals **10** are significantly raised in energy with respect to orbitals **11**, so that orbital mixing of **10** into **11** is diminished. That is, the lowering of band orbitals **11** by **10** is strongly reduced in real chain **3**. Therefore bands b_+ and b_- become more dispersive in **3** than in **4**. Bands b_+ and b_- represent primarily through-bond interactions between metal atoms in each subchain of **3**.

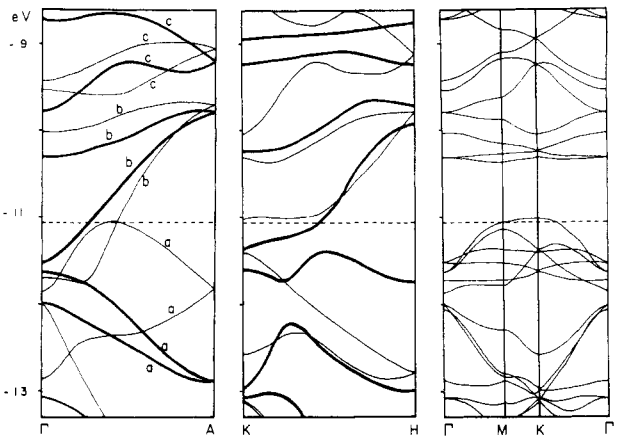

Figure 2. Low-lying d-block bands of Nb_3S_4: (a) along the chain direction $\Gamma \rightarrow A$; (b) along the chain direction $K \rightarrow H$; (c) along several directions perpendicular to the chain direction. The Fermi level for Nb_3S_4 is shown by the dashed line.

B.3. Nb_3S_4. Figure 2a shows the t_{2g} subbands of Nb_3S_4 along the chain direction $\Gamma \rightarrow A$ (see **12** for the definition of some special points of the first Brillouin zone), where thick and thin lines

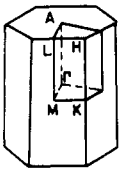

12

represent doubly and singly degenerate bands, respectively. Nb_3S_4 has three zigzag Nb chains and thus six Nb atoms per unit cell, so that there occur 18 t_{2g} subbands. Comparison of Figures 1b and 2a reveals that Nb_3S_4 has three sets of six bands (labeled as a, b, and c in Figure 2a) derived essentially from the three pairs of bands (i.e.: a_+ and a_-; b_+ and b_-; c_+ and c_-) of real chain **3**. This is due to the fact that the zigzag Nb chains in Nb_3S_4 interact weakly via bridging sulfur atoms.

With the formal oxidation state of S^{2-}, there remain 14 d electrons per unit cell Nb_6S_8. Thus the six a bands of Figure 2a are completely filled, which gives rise to six formal Nb–Nb single bonds per unit cell (i.e., two Nb–Nb single bonds per zigzag Nb chain). The remaining two d electrons now fill the bottom portion of bands b. Our calculations show that, in every zigzag Nb chain of Nb_3S_4, the overlap population of each Nb–Nb bond across the two subchains is 0.26, while that of each short Nb–Nb contact within a subchain is 0.07. Thus, between metal atoms of every zigzag Nb chains, bonding interactions occur primarily across the subchains as suggested by the short Nb–Nb bond length of 2.88 Å, but those along each subchain are not negligible despite the long Nb–Nb distance of 3.37 Å. For a triangular Nb cluster of Nb_3S_4, in representation **1**, the overlap population is 0.04 between Nb atoms, which is the weakest among all nearest-neighbor Nb–Nb contacts. Therefore, structural representation **2** is more appropriate than **1** for the description of the electronic structure of Nb_3S_4.

The band electronic structure of Nb_3S_4 calculated along other directions of the first Brillouin zone are shown in Figure 2b,c. It is noted that our results on Nb_3S_4 are very similar to those obtained by Oshiyama in terms of self-consistent-field calculations.[5a,b] Figure 3 shows the density of states (DOS) calculated for Nb_3S_4.[11]

(10) (a) Whangbo, M.-H. *Crystal Chemistry and Properties of Materials with Quasi One-Dimensional Structures*; Rouxel, J., Ed.; Reidel: Dordrecht, The Netherlands, 1986, p 27. (b) Whangbo, M.-H.; Foshee, M. J. *Inorg. Chem.* **1981**, *20*, 113. (c) Shaik, S.; Hoffmann, R.; Fisel, C. R.; Summerville, R. H. *J. Am. Chem. Soc.* **1980**, *102*, 4555.

(11) A set of 36 special k-points[15] in the irreducible portion of the first Brillouin zone (see **12**) was used to calculate DOS and overlap populations.

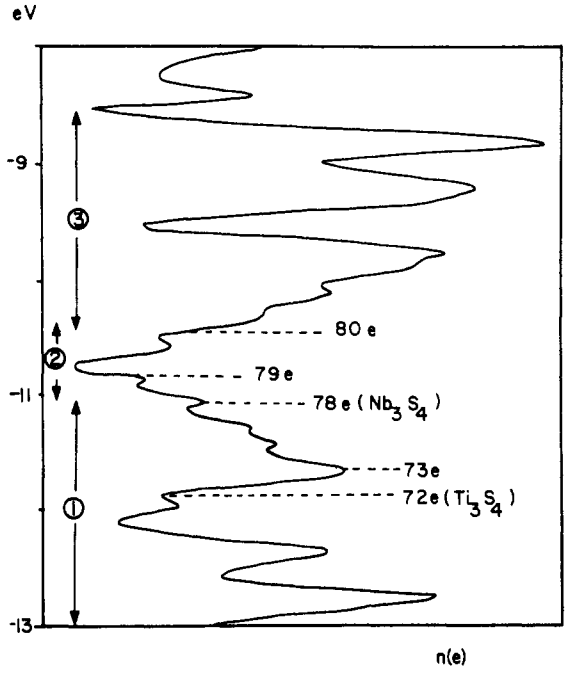

Figure 3. Density of states calculated for Nb_3S_4. A number of dashed lines indicate the Fermi levels corresponding to different numbers of electrons per unit cell in the Nb_3S_4 or the Ti_3S_4 lattice.

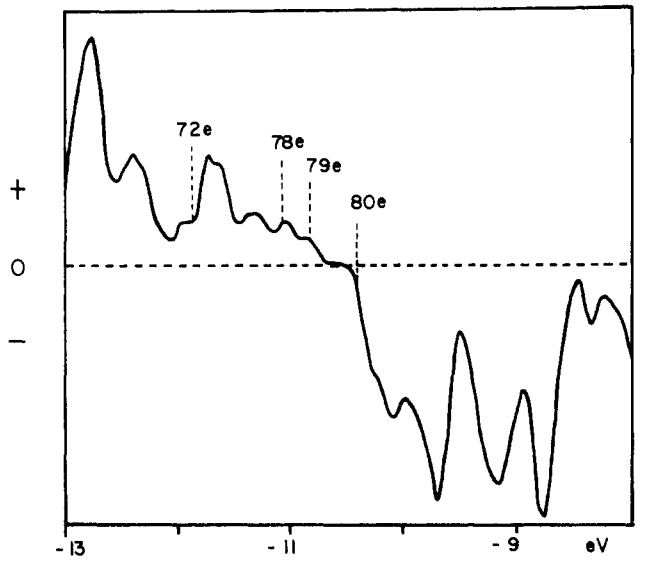

Figure 4. Overlap population of the Nb–Nb bond in the zigzag chains of Nb_3S_4 as a function of energy.

In agreement with other calculations,[5] the Fermi level of Nb_3S_4 lies near a minimum of the DOS curve. As can be deduced from Figures 1b and 2a, this arises from the partially filled b bands that are somewhat dispersive.

Figure 4 shows how the overlap population of an Nb–Nb bond in each zigzag Nb chain varies as a function of energy. This bond is found to be antibonding beyond −10.5 eV. Comparison of Figures 3 and 4 reveals that energy region 1 (−13 to −11 eV), where the six a bands occur, represents bonding between Nb atoms across two subchains. Energy region 3 (−10.5 to −8.5 eV), where all c bands and the upper portion of b bands occur, represents antibonding between metal atoms across two subchains. Regions 1 and 3 contain high DOS peaks since the bonding and antibonding bands describing the Nb–Nb bonds across subchains are relatively flat. Energy region 2 (−11 to −10.5 eV) has small DOS values, since this region is mainly represented by the lower portion of b bands that are relatively dispersive.

The $n(e_f)$ values of Nb_3X_4 (X = S, Se, Te) compounds are calculated to be small (e.g., $n(e_f)$ = 2.20, 3.17, and 2.28 states/eV per formula unit Nb_3X_4 for X = S, Se, and Te, respectively[5a,b]). Nevertheless, all Nb_3X_4 compounds exhibit superconductivity (T_c = 4.0, 2.0, and 1.8 K for Nb_3S_4, Nb_3Se_4, and Nb_3Te_4, respectively).[2] The $n(e_f)$ values of the Nb_3X_4 lattice may be modified by intercalation of Nb_3X_4 with alkali metals A. In an intercalated compound $A_xNb_3X_4$, alkali-metal cations A^+ reside in the hexagonal channels while the Nb_3X_4 lattice receives the electrons given up by A (i.e., $2x$ electron per unit cell Nb_6X_8). According to Figure 3, this intercalation would lead to very small values of $n(e_f)$ for $0 < x < 0.8$.[12] Alkali-metal intercalation changes the Fermi level of the Nb_3X_4 lattice, which could lead to interesting changes in the Fermi surface and hence in the nesting condition. One way to increase the $n(e_f)$ value of the Nb_3X_4 lattice is to remove electrons from it. From this viewpoint, it is of interest to consider the Ti_3X_4 (X = S, Se) lattice of $A_xTi_3X_4$,[4] which has a crystal structure similar to that of Nb_3X_4. Thus the DOS curve of Ti_3X_4 may be approximated by that shown in Figure 3. Ti_3X_4 has six electrons less per unit cell than does N_3X_4, so that the $n(e_f)$ value expected for Ti_3X_4 is small. However, for the Ti_3X_4 lattice of $A_xTi_3X_4$, the $n(e_f)$ value can be found at a high-DOS peak. According to Figure 3, a high $n(e_f)$ value can be obtained for $A_xTi_3X_4$ with $x \cong 0.5$.[12] Thus, examination of physical properties of $A_xTi_3X_4$ as a function of x would be very interesting if such properties are sensitive to the $n(e_f)$ values.

Concluding Remarks

Nb_3X_4 consists of zigzag Nb chains, which are linked together via chalcogen atoms X. The bonding character associated with each zigzag Nb chain is well described by real Nb_2X_6 chain **3**, which is a distorted structure of ideal Nb_2X_6 chain **4**. The latter results when two NbX_4 chains **5** are fused together by sharing four edges. Our band electronic structure calculations show that the low-lying d-block bands of Nb_3X_4 are essentially derived from the t_{2g} subbands of **3**, whose character can be easily traced to the t_{2g} subbands of **4** upon considering the distortion **4** → **3**. Thus we were able to show why the Fermi level of Nb_3X_4 lies near a minimum of the DOS curve. Based upon the present calculations, it was speculated that the $n(e_f)$ value and the Fermi surface of the Nb_3X_4 lattice in $A_xNb_3X_4$ as well as the Ti_3X_4 lattice in $A_xTi_3X_4$ can be significantly modified by changing the extent of alkali-metal intercalation.

Acknowledgment. This work was in part supported by the Camille and Henry Dreyfus Foundation through a Teacher-Scholar Award (1980–1985) to M.-H.W., which made it possible for E.C. to visit the Department of Chemistry, North Carolina State University.

Registry No. Nb_3S_4, 12266-24-9; Nb_2S_6, 12316-04-0.

(12) Besides inherent lattice defects, the extent of alkali-metal intercalation in Nb_3X_4 and Ti_3X_4 lattices depends upon the size of alkali-metal cation A^+. For example, $x \simeq 1$, 0.2, 0.2 for A = Li, Na, K in $A_xNb_3S_4$, respectively, and $x \simeq 0.8$, 0.3 for A = Li, K in $A_xTi_3S_4$.[4]
(13) Basch, H.; Gray, H. B. *Theor. Chim. Acta* **1966**, *4*, 367.
(14) Ammeter, J. H.; Bürgi, H.-B.; Thibeault, J. C.; Hoffmann, R. *J. Am. Chem. Soc.* **1978**, *100*, 3686.
(15) (a) Chadi, D. J.; Cohen, M. L. *Phys. Rev. B: Solid State* **1973**, *8*, 5747. (b) Monkhorst, H. L.; Pack, J. D. *Phys. Rev. B: Solid State* **1976**, *13*, 5188. (c) Baldereschi, A. *Phys. Rev. B: Solid State* **1973**, *7*, 5212.